Review on laminar flame speed and its measurement from outwardly propagating spherical flames

Mahdi Faghih[1] & CHEN Zheng (陈正)[1,2*]

[1] *State Key Laboratory for Turbulence and Complex Systems (SKLTCS), Department of Mechanics and Engineering Science, College of Engineering, Peking University, Beijing 100871, China;*

[2] *Center for Applied Physics and Technology (CAPT), Beijing Innovation Center for Engineering Science and Advanced Technology (BIC-ESAT), Peking University, Beijing 100871, China*

Received September 18, 2018; accepted November 20, 2018

Abstract The laminar flame speed is one of the most fundamental properties of a fuel/air mixture. It determines the fuel burning rate in combustion engines and is an important target used to validate chemical models. Due to its importance, accurate measurement of the laminar flame speed receives great attention and different experimental methods have been developed. This review first introduces the laminar flame speed as well as its significance and dependence on different factors. Then, different experimental methods for the laminar flame speed measurement are described. Since the outwardly propagating spherical flame method is currently the most popular method for laminar flame speed measurement, its challenges and recent advances are reviewed. Both the constant pressure method and constant volume method using propagating spherical flames are discussed.

Keywords Laminar flame speed; Propagating spherical flame; Constant pressure method; Constant volume method.

doi: 10.16262/j.cnki.1005-0841.2018.04.002

1 Introduction

Longman Contemporary Dictionary [1] defines the combustion as "chemical activity which uses oxygen to produce light and heat". Combustion is currently the major method of energy production and conversion. The fossil fuels and biofuels used in combustion consist of the primary source of energy supply. Although strict policies are implemented to control the pollution generated by combustion, energy conversion through combustion of fossil fuels will remain to be dominant in energy supply in the near future [2].

Usually the combustion process is accompanied by flames. Depending on how the fuel and oxidizer are prepared, there are two types of flames, namely, the premixed flame and non-premixed flame. In the premixed flame, the reactants are mixed before chemical reactions occur. One important characteristic of the premixed flame is that it can be regarded as a wave propagation at a specific speed. For each fuel/oxidizer mixture at given pressure and temperature, the laminar premixed flame has a unique propagation rate, characterized by the so-called laminar flame speed (LFS) or laminar burning velocity (LBV). This review focuses on the laminar flame speed and its measurement.

* Corresponding author (Email: cz@pku.edu.cn; Tel: 86-10-62766232)

2 Laminar flame speed

2.1 Definition and significance of the laminar flame speed

The laminar flame speed (LFS), S_u^0, is a fundamental property of a combustible mixture. It is defined as the speed at which a planar, unstretched, adiabatic, premixed flame propagates relative to the unburned mixture [3]. The schematic of the one-dimensional premixed flame propagation is shown in Fig. 1. In the coordinate attached to the flame front, the flow speed of the unburned mixture is equal to S_u^0. The products leave the reaction zone at the speed of S_b^0, which is much larger than S_u^0 due to thermal expansion.

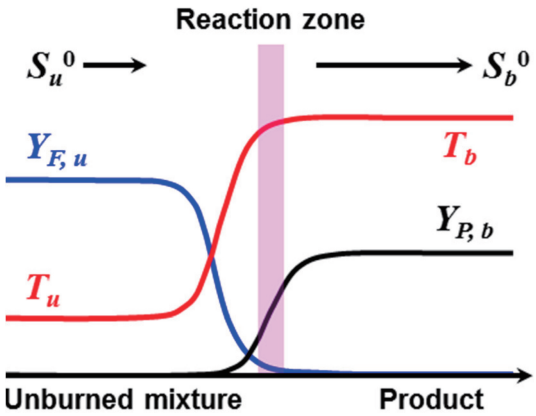

Figure 1 Schematic of one-dimensional premixed planar flame propagation.

LFS is a unique property of a combustible mixture. Many premixed flame phenomena, such as extinction, flash back, and blow off can be characterized by LFS [4]. In internal combustion engines, LFS affects the fuel burning rate and the engine performance [5]. In fundamental combustion research, the LFS is an important target which is used to validate chemical mechanisms and to develop surrogate fuel models (e.g. [6—8]). Recently, accurate measurement of LFSs at high pressures and temperatures has become extremely important for the development and validation of chemical mechanisms of gasoline, diesel, and jet surrogate fuels. Furthermore, the LFS is used in certain turbulent premixed combustion modeling within the flamelet regime [9].

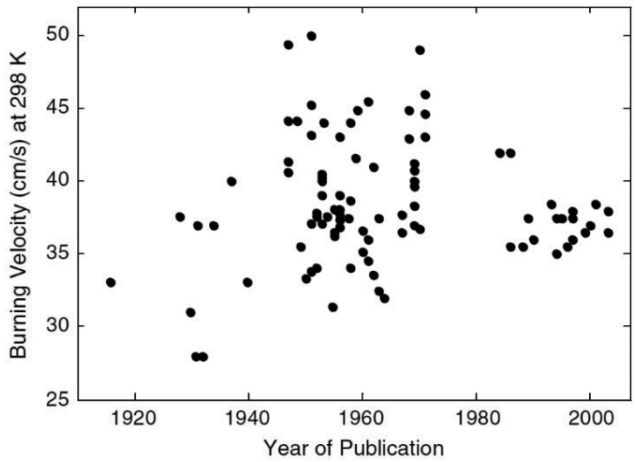

Figure 2 The maximum LFS measured for the methane/air mixture at $T_u = 298$ K and $P = 1$ atm. Figure adapted from Ref. [10].

Despite the simple definition of LFS, accurately measuring LFS is challenging. Fig. 2 shows the reported maximum LFS measured for methane/air at normal temperature and pressure (NTP, 298 K and 1 atm) over the years. Although the data scatter becomes weaker after the introduction of aerodynamic

stretch effect [4] in the early 1980s, the relative difference between the reported data is still significant. Since accurate measurement of LFS is extremely important for constraining the uncertainty of chemical models, substantial attention (e. g., [11—22]) has been devoted to improving the accuracy of LFS measurement.

2.2 Dependent factors affecting the laminar flame speed

Different factors including the adiabatic flame temperature, thermal conductivity, molecular structure, pressure and initial temperature affect the LFS [4]. Simple analysis yields the following correlation for LFS [4]:

$$S_u^0 \sim P^{(n/2-1)} \sqrt{\lambda/C_P} \cdot \exp(-E_a/2T_{ad}), \tag{1}$$

where P is the pressure, n the overall reaction order, λ the thermal conductivity, C_P the specific heat capacity, E_a the activation energy and T_{ad} the adiabatic flame temperature.

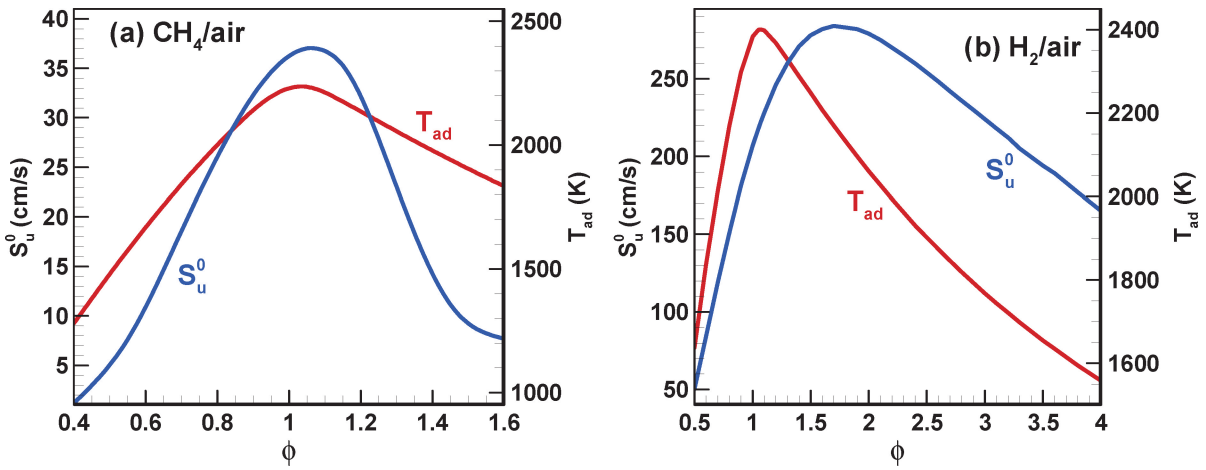

Figure 3 Calculated adiabatic flame temperature, T_{ad}, and LFS, S_u^0, of methane/air (a) and hydrogen/air (b) at $T_u = 298$ K and $P = 1$ atm. The GRI-Mech 3.0 [23] and the mechanism developed by Li et al. [24] are used respectively for methane/air and hydrogen/air.

Specifically, the adiabatic flame temperature influences the reaction rate and thus the LFS as shown in Eq. (1). Fig. 3(a) shows the adiabatic flame temperature and LFS of the methane/air mixture at $T_u = 298$ K and $P = 1$ atm. It is seen that the two curves have the same shape and both peak at the near-stoichiometric position. Fig. 3(b) shows the results for hydrogen/air mixtures. There is a shift in the peak of the LFS (around $\phi = 1.75$) from that of the adiabatic flame temperature (around $\phi = 1.07$). This is due to the large thermal conductivity of hydrogen which affects the LFS according to Eq. (1). Equation (1) indicates that the LFS is proportional to the square root of the Lewis number (Le), which is the ratio between thermal diffusivity (α) and mass diffusivity (D) of the deficient reactant. Since Le of a hydrogen/air mixture changes from 0.33 to 2.3 for fuel-lean to fuel-rich conditions, the effect of Le is to reduce the LFS on the fuel-lean side and to increase it on the fuel-rich side [4].

Fig. 4 shows the effect of pressure on LFS for methane/air and hydrogen/air mixtures. According to Eq. (1), the LFS decreases with the pressure since the overall reaction order is usually in the range of $1 < n < 2$ [4]. The LFS increases monotonically with the initial temperature, which is shown in Fig. 5 for a stoichiometric methane/air mixture. This is mainly because the adiabatic flame temperature increases with the initial temperature. According to Ref. [25], the LFS of normal alkanes of C_5—C_{12} is mainly affected by the chemistry for H_2/CO and C_1—C_4. Therefore, the carbon number is expected to have little influence on the LFS. This is demonstrated by Fig. 6, which shows that for all of the alkanes except methane, the LFS does not change strongly with carbon number.

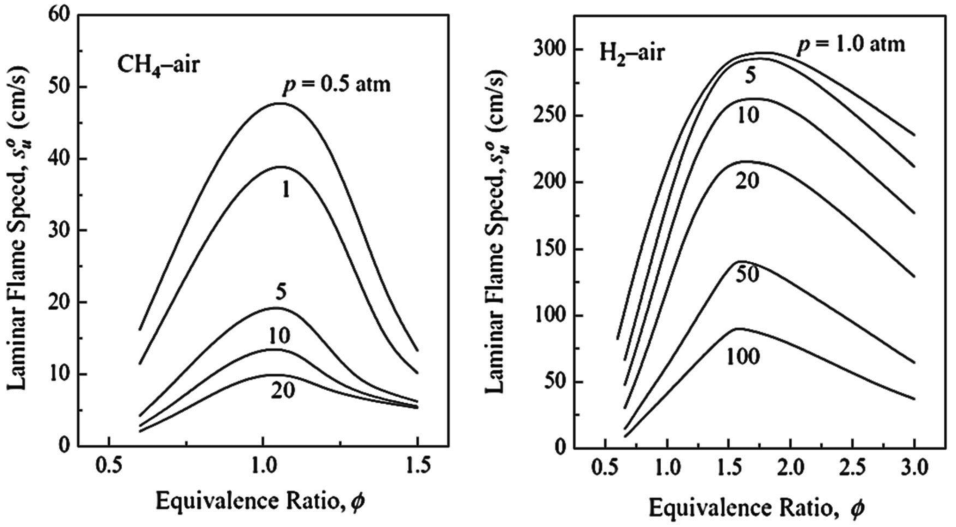

Figure 4 Calculated LFS of methane/air (left) and hydrogen/air (right) at different initial pressures. Figure adapted from Ref. [4].

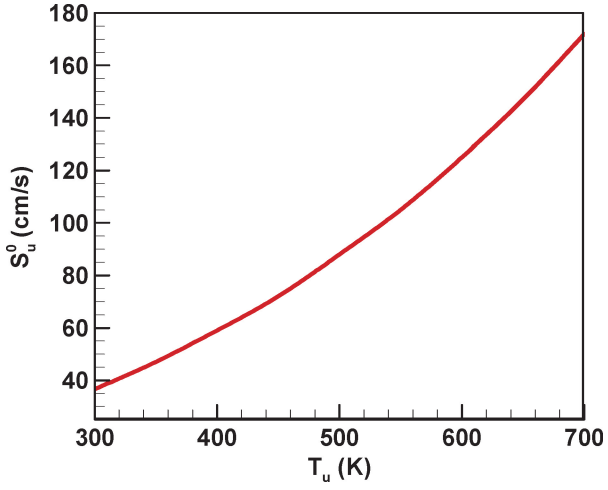

Figure 5 Calculated LFS as a function of initial temperature for stoichiometric methane/air at $P=1$ atm. The GRI-Mech 3.0 [23] is used for simulation.

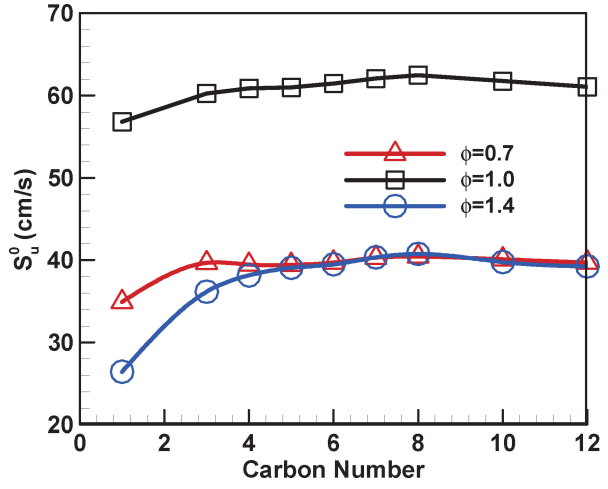

Figure 6 Change of LFS with carbon number for the stoichiometric normal-alkane/air mixture at $T_u=400$ K and $P=1$ atm calculated by PREMIX [26].

2.3 Methods for laminar flame speed measurement

Due to the importance of LFS, great attention has been paid to its *accurate* measurement. Different experimental approaches have been developed to measure LFS using different flame configurations, including the Bunsen flame [27], the counter flow or stagnation flame [28—31], the burner stabilized flat flame [32, 33], and the outwardly propagating spherical flame [5, 27, 34—50].

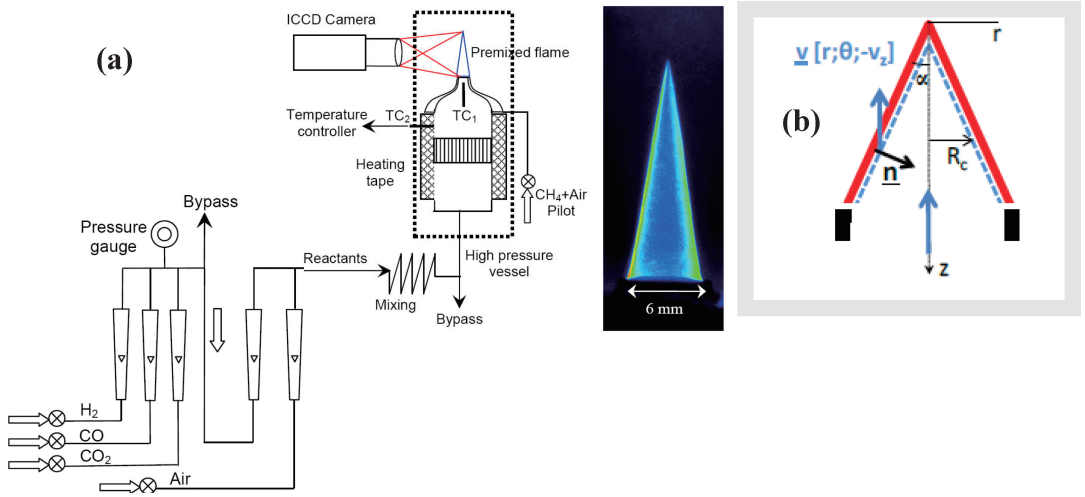

Figure 7 Schematic of the Bunsen flame configuration (a) and flame structure (b). Figure (a) from [51] and Figure (b) adapted from [52].

Bunsen flames were used to measure the LFS in 1866 [53]. The schematic of the Bunsen flame experiment is shown in Fig. 7(a). This method is popularly used due to its simplicity. In a Bunsen flame, the volumetric flow rate at the burner exit and the flame shape can be directly measured. According to Fig. 7(b), the LFS can be determined as $S_u^0 = V_z \sin\alpha$, in which V_Z is the inlet flow speed and α is the cone angle.

Several assumptions are made to measure the LFS from Bunsen flames, including constant flame speed along the flame surface, negligible stretch effects, and infinite thin flame front. However, Bunsen flames can be affected by instability, negative stretch rate and strong curvature effect around flame tip [54, 55]. Bunsen flames were continuously adapted to measure the LFS [56—58] and usually the stretch effects were neglected [59]. Its accuracy is lower than that of the counter flow flame method and the propagating spherical flame method introduced below.

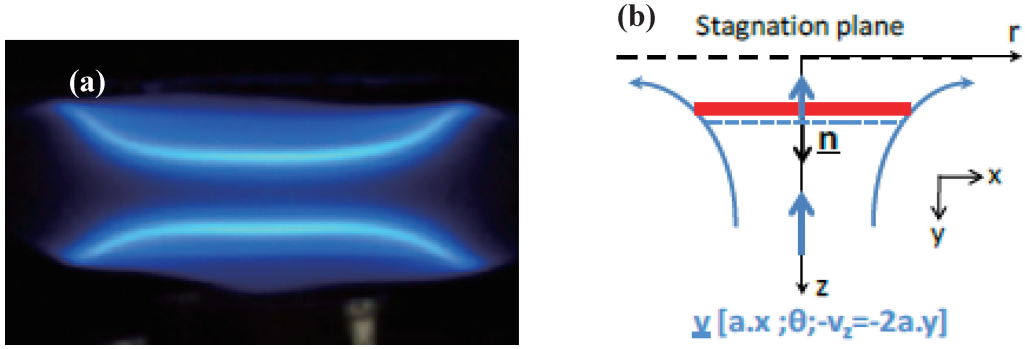

Figure 8 The counter flow flame: (a) twin flames; (b) schematic of flame and flow. (a) is from [59] and figure (b) from [52].

Counter flow flames or stagnation flames were introduced in 1957 [60]. Wu and Law [29] used this method to measure the LFS with stretch correction. The twin flames and schematic of flame and flow are shown in Fig. 8. Due to the symmetrical geometry of the counter flow flame, there is no downstream conductive heat loss. As a result, the flame is only affected by stretch rate due to non-uniform external

flow. In counter flow flames, there are three zones: the hydrodynamic zone, preheat zone and reaction zone. In the hydrodynamic zone, the flow decelerates after leaving the burner nozzle exit and before entering the preheat zone. Then the flame accelerates due to thermal expansion in the preheat and reaction zones. It decelerates again near the stagnation plane. To obtain the flame speed, two parameters both in the hydrodynamic zone are measured. The first one is the maximum axial velocity gradient which is used to calculate the stretch rate; and the second one is the minimum reference flame speed. It is noted that the minimum reference flame speed is not the same as the LFS. Finally, linear or nonlinear extrapolation can be performed to obtain the unstretched LFS. It is noted that there are extrapolation errors especially for large hydrocarbon fuels in fuel rich conditions [61]. The uncertainty of the method is around ±5%. The most restricting factor of using this method is the narrow pressure range of 0.1—5 atm [59]. It's difficult to use this method for pressure above 5 atm, under which the flat flame is difficult to be maintained.

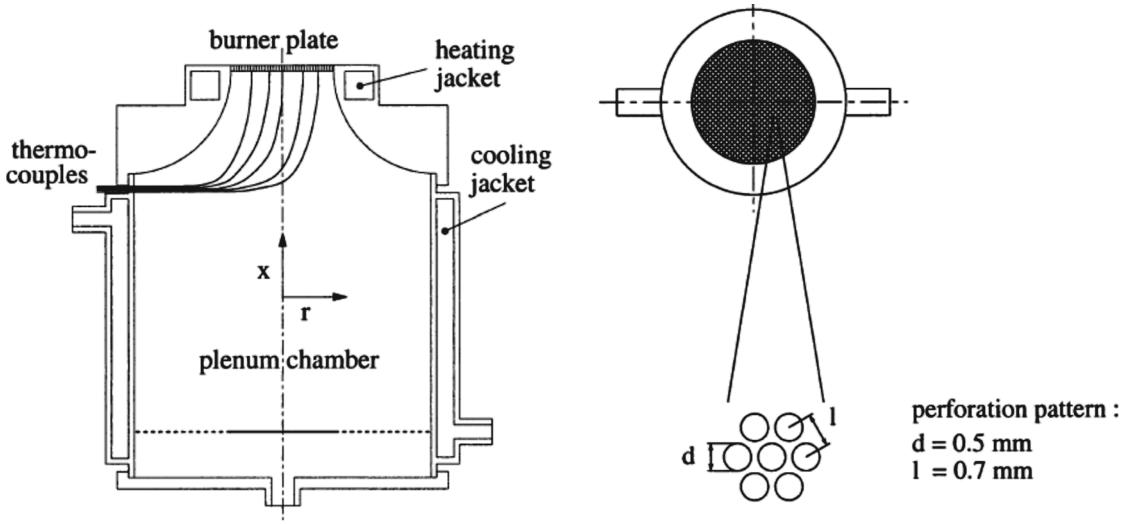

Figure 9 Left: schematic of the heat flux burner. Right: perforation pattern from the top. Figure from Ref. [62].

The heat flux method was proposed by Botha and Spalding [63] and was further developed by de Goey et al. [64]. The schematic of heat flux burner is shown in Fig. 9. The method was originally developed based on the fact that the heat loss to the burner depends on free stream velocity; and the LFS can be determined by linear extrapolation to zero heat loss. To simplify the procedure the stability was retained by spherical and cylindrical porous burners in which flow divergence replaced heat loss to maintain stability [65]. The challenge raised from using porous burners is to maintain the 1D symmetry of the flame, which requires a micro-gravity environment. In order to diminish the heat loss effects, de Goey et al. [64] proposed the updated version of the heat flux method. The idea is to provide additional heat to the unburned mixture to compensate the heat loss from the flame to the burner surface. Alekseev et al. [66] reviewed the uncertainties of the heat flux method. According to [66], asymmetric heat flux, the flow uniformity on edges, unburned gas temperature, pressure and the calibration of the mass flow controllers are the main sources of uncertainty in the heat flux method. It is noted that the LFS measurements by the heat flux method were mainly conducted at atmospheric pressure and only a few experiments were conducted at 200 mbar [67] and 5 atm [33]. Similar to the counter flow flame method, the heat flux method is difficult to be used for pressure above 5 atm.

The advantages and disadvantages of these methods mentioned above are summarized in Table 1. Those for the propagating spherical flame method which will be discussed in the next section are also presented in Table 1 for comparison. It is seen that only the propagating spherical flame method can be used to determine the LFS at elevated pressures and temperatures close to engine conditions.

Table 1 The advantages and disadvantages of different methods used to measure the LFS

Method	Advantages	Disadvantages
The Bunsen flame	It has simple and flexible experimental setup.	Wall quenching effects exist in experiments. Curvature and strain effects are usually not corrected. It does not work at elevated pressures.
The counter flow flame	The heat loss can be diminished. Stretch effects can be corrected.	There is multi-dimensional effect. It does not work at elevated pressures.
The heat flux method	The flame is unstretched and nearly adiabatic. Aerodynamic straining has a stabilizing effect for cellular instabilities.	A reference plane should be chosen: ambiguity of interpretation for the flame strain sensitivity. It does now work at elevated pressures.
The propagating spherical flame	The flame is one-dimensional. Stretch effects can be corrected. It can be used for a broad range of pressures and temperatures.	Extrapolation to zero stretch rate is required. For weakly burning flames, the flame can be distorted due to buoyancy effects.

3 Propagating spherical flame method for LFS measurement

The propagating spherical flame method was introduced by Stevens as the soap bubble method in 1926 [68]. In this method, a spherical flame propagates outwardly after central spark ignition in the quiescent homogeneous combustible mixture [27, 35]. Either the pressure history or the flame front history is recorded, based on which the LFS is determined. The advantages and disadvantages of this method to measure LFS are compared with other methods in Table 1. As can be seen in the table, the propagating spherical flame method is the only method to measure the LFS at a wide range of pressures and temperatures.

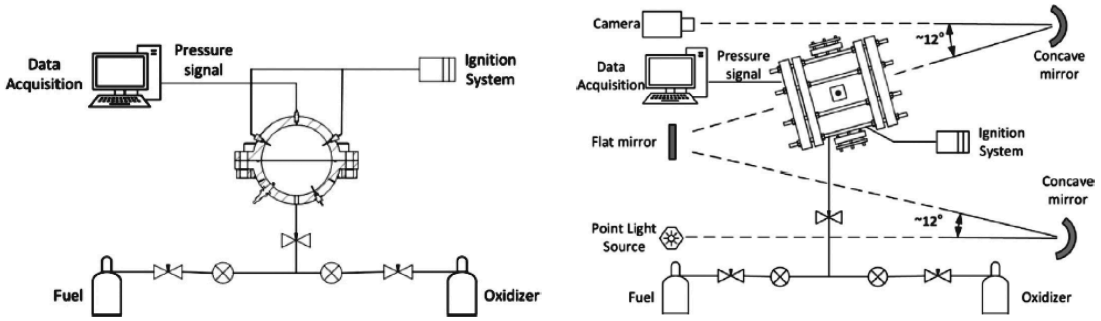

Figure 10 Schematic of the spherical chamber configuration with pressure transducer (left) and the cylindrical chamber configuration with optical access (right) to determine the LFS using the propagating spherical flame method. Figure adapted from [69].

The schematic of experimental facility by which the flame front history and pressure history are recorded are shown in Fig. 10. At the early stages of flame propagation, the flame stretch effects are strong while the pressure rise is negligible. Later the pressure rise rate increases greatly while the curvature/stretch effects become negligible [21]. Depending on the chamber design as well as the pressure rise, there are two different methods for LFS measurement by using propagating spherical flames: the constant pressure method (CPM) and the constant volume method (CVM). Fig. 11 schematically describes and compares these two methods. As indicated by the dashed ellipses in Fig. 11, flames with small radii (e.g., $1 \leqslant R_f \leqslant 2$ cm) are used in CPM so that the pressure rise is negligible. In CVM, data corresponding to relatively large flame radii are used since discernible pressure rise is required. In the following, the CPM and CVM are discussed separately.

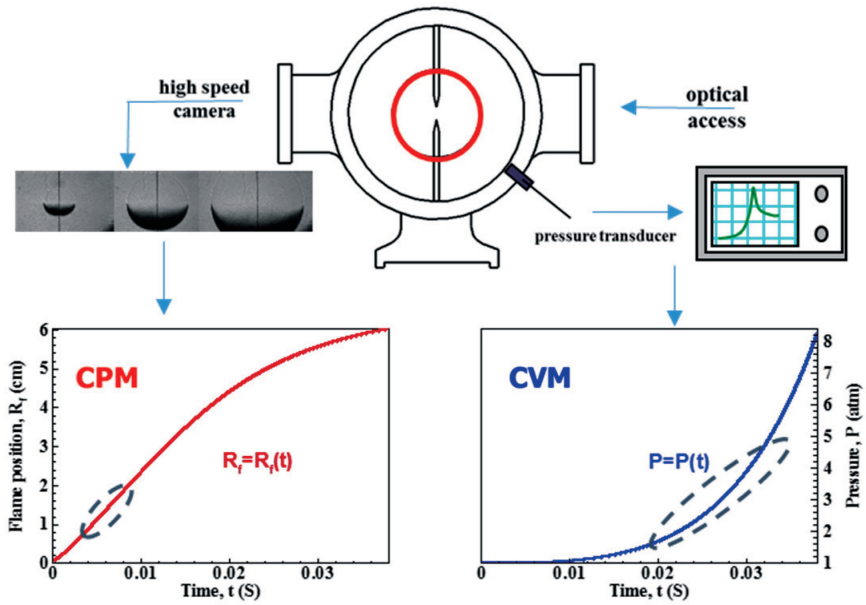

Figure 11 Schematic for the constant pressure method (CPM) and constant volume method (CVM) using propagating spherical flames. Figure adapted from [70].

3.1 Constant pressure method (CPM)

The propagating spherical flame experiment with optical access in a spherical chamber was first conducted by Ellis [71], who used the glass spherical chamber to study the confinement effect on flame propagation. In the constant pressure method (CPM), Schlieren or shadow photograph is used to record the flame front propagation history. In CPM, the following assumptions are made to determine the LFS [59]: 1) the pressure remains to be constant during the flame propagation; 2) the unburned gas is compressed isentropically; 3) the burned gas is stagnant and under the thermodynamic equilibrium condition; 4) the flame is spherical and there is no thermo-diffusive or hydrodynamic instability; 5) the ignition energy is small and it does not influence the flame trajectory.

As shown in Fig. 11, in the early stages of a flame propagation the pressure rise is negligible, and thereby zero burned gas velocity is usually assumed (i. e., $U_b=0$). Consequently, the propagating speed of the experimentally visualized flame front is equal to the flame speed with respect to the burned mixture:

$$S_b = \frac{\mathrm{d}R_f}{\mathrm{d}t} - U_b = \frac{\mathrm{d}R_f}{\mathrm{d}t}, \tag{2}$$

where R_f is the flame radius; U_b is the burned gas velocity; and S_b is the laminar flame speed with respect to the burned gases. However, the propagation velocity measured at the early stages of flame propagation is affected by the positive stretch effect. For an outwardly propagating spherical flame, the flame stretch is [27]:

$$K = \frac{1}{A}\frac{\mathrm{d}A}{\mathrm{d}t} = \frac{2}{R_f}\frac{\mathrm{d}R_f}{\mathrm{d}t}, \tag{3}$$

where $A=4\pi R_f^2$ is the area of the flame front. In the 1980s, the concept of stretch effect was well recognized [59]. The stretch effect modifies the flame speed by preferential diffusion of heat and deficient reactant, which is quantified by the Lewis number (Le). Therefore, for accurate determination of the LFS, it is necessary to eliminate the stretch effect by extrapolation of the flame speed to zero stretch.

Usually the following linear model is used to obtain the unstretched flame speed:

$$S_b = S_b^0 - L_b K, \tag{4}$$

where S_b^0 and L_b are respectively unstretched LFS and Markstein length with respect to the burned gas. Numerical differentiation is required to calculate S_b and K. It can be avoided by integrating Eq. (4) into:

$$R_f = S_b^0 t - 2L_b \ln(R_f) + cte. \tag{5}$$

Kelley and Law [72] found strong nonlinearity between the propagation speed and flame stretch. They suggested to use the following nonlinear model to determine S_b^0:

$$\left(\frac{S_b}{S_b^0}\right)^2 \ln\left(\frac{S_b}{S_b^0}\right)^2 = \frac{-2L_bK}{S_b^0}. \tag{6}$$

Chen [18] suggested the following linear relationship between S_b and curvature:

$$S_b = S_b^0 - kL_bS_b^0, \tag{7}$$

where $k=2/R_f$ is the curvature. Chen [18] showed that while Eq. (6) is the most accurate model for mixtures with small Lewis number, for mixtures with large Lewis number Eq. (7) is more accurate. When the Lewis number is close to unity, Eq. (4) can be used. In the formulation introduced above, the flame thickness is neglected in LFS determination. Recently, Liang et al. [73] proposed to consider the flame thickness using the following correlation:

$$\left(\frac{S_b}{S_b^0}+\frac{2\delta}{R_f}\right)\ln\left(\frac{S_b}{S_b^0}+\frac{2\delta}{R_f}\right)=\frac{-2(L_b-\delta)}{R_f} \tag{8}$$

where δ is the flame thickness. It is noted that for the limiting case of $2\delta/R_f\to 0$, Eq. (8) degenerates into Eq. (6). It was shown in [73] that Eq. (8) is more accurate to determine the LFS than other formulations for lean hydrogen/air and rich n-heptane/air mixtures. Other formulations were also proposed by different research groups to determine the unstretched LFS [74, 75]. These extrapolation equations are summarized in Table 2.

Table 2 Extrapolation equations to obtain unstretched LFS

Reference	Formulation
[29]	$S_b = S_b^0 - L_bK$
[72]	$\left(\frac{S_b}{S_b^0}\right)^2 \ln\left(\frac{S_b}{S_b^0}\right)^2 = \frac{-2L_bK}{S_b^0}$
[18]	$S_b = S_b^0 - kL_bS_b^0$
[74]	$\frac{S_b}{S_b^0}\left[1+\frac{2L_b}{R_f}+\frac{4L_b^2}{R_f^2}+\frac{16L_b^3}{3R_f^3}+o^4\left(\frac{L_b}{R_f}\right)\right]=1$
[75]	$\frac{S_b}{S_b^0}=1-\frac{2L_b}{R_f}+\frac{C}{R_f^2}$
[73]	$\left(\frac{S_b}{S_b^0}+\frac{2\delta}{R_f}\right)\ln\left(\frac{S_b}{S_b^0}+\frac{2\delta}{R_f}\right)=\frac{-2(L_b-\delta)}{R_f}$

Once S_b^0 is determined, the unstretched LFS with respect to unburned gas, S_u^0 can be obtained by applying mass conservation:

$$S_u^0 = \frac{\rho_bS_b^0}{\rho_u} \tag{9}$$

where ρ_u and ρ_b are the density of unburned and burned gas, respectively.

Recently a new method was proposed and used by Renou and coworkers [13, 76, 77]. The LFS is directly measured by recording the flame propagation speed ($S=\mathrm{d}R_f/\mathrm{d}t$) and the unburned gas velocity near the preheat zone of the flame front,

$$S_u^0 = S - U_u \tag{10}$$

where U_u is the unburned gas velocity near the flame front and it is measured through the particle image velocimetry (PIV) method. This method has the advantage over the conventional method since the density ratio and the assumption of zero burned gas velocity are not required.

There are two main advantages of the CPM method. First, the flame surface is observed and recorded during the whole period of propagation. Therefore, instability in the flame can be observed and analyzed. Second, the pressure and temperature rise is negligible during early stages of the flame propagation and thereby the flame is only affected by stretch, which allows the extrapolation to zero stretch and determination of stretch effect [21]. However, because of the requirement of optical access, the upper-pressure limit of CPM is usually lower than that of CVM. Dual chambers have been used to develop the

pressure-release type high-pressure combustion facilities [34, 38] and pressures up to 60 atm have been reached for the CPM. Compared to CVM, the main drawback of CPM is its relatively low-temperature ranges [69]. It is difficult to conduct spherical flame experiments by CPM at temperature and pressure close to engine-relevant conditions [69]. However, the CPM is popularly used to measure the LFS. It is used by many groups such as Halter and coworkers [44, 78—81], Pitsch and coworkers [12, 82—84], Law and coworkers [38, 72, 85, 86] and Renou and coworkers [13, 14, 76, 77].

Table 3 summarizes different groups using CPM to measure the LFS.

Table 3 The CPM experiments conducted by different groups to measure LFS

Group	Vessel type and size
Halter and coworkers [78, 79, 81]	cylindrical, $R_w=16$ cm, $L=30$ cm
Halter et al. [44]	spherical, $R_W=12.5$ cm
Brequigny et al. [80]	spherical, $R_W=20$ cm
Pitsch and coworkers [12, 82—84]	spherical, $R_W=5$ cm
Bradley and coworkers [41, 87]	spherical, $R_W=19$ cm
Faeth and coworkers [36, 40, 88, 89]	spherical, $R_W=18$ cm
Qiao et al. [90]	spherical, $R_W=18$ cm in microgravity
Law and coworkers [38, 72, 85, 86]	cylindrical, $R_W=4.12$ cm, $L=12.7$ cm
Ju and coworkers [34, 91]	cylindrical, $R_W=5$ cm, $L=15.24$ cm
Kim et al. [92]	spherical, $R_W=10$ cm
Renou and coworkers[13, 14, 76, 77]	spherical, $R_W=8.5$ cm
Kuznetsov et al. [93]	spherical, $R_W=12.5$ cm
Farrel et al. [94]	spherical, $R_W=8.25$ cm
Daly et al. [95]	spherical, $R_W=12.5$ cm
Peters and coworkers [96, 97]	spherical, $R_W=5$ cm
Takizawa et al. [45, 98]	spherical, $R_W=9$ cm
Fluixá et al. [99]	cylindrical, $R_W=15.25$ cm and $L=30.5$ cm
Pizzuti et al. [100]	cylindrical, $R_W=7.5$ cm and $L=15$ cm
Hinton et al. [101]	spherical, $R_W=8$ cm

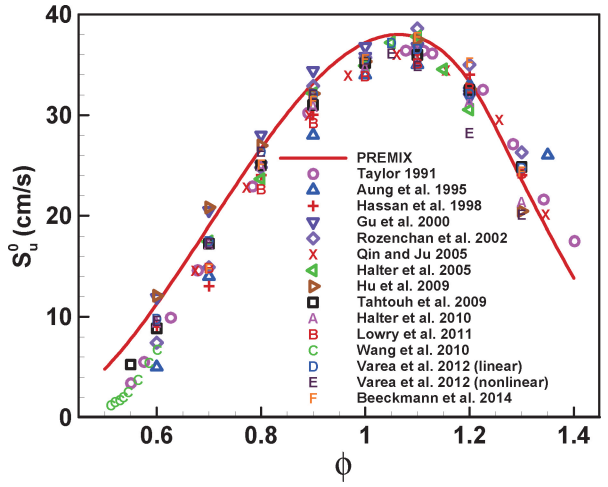

Figure 12 LFS measured by CPM for the methane/air mixture at $T_u=298$ K and $P=1$ atm. Symbols and lines respectively denote the experimental and numerical results obtained by PREMIX. Figure adapted from [16].

The LFS of methane/air at NTP measured by different groups using the CPM are shown in Fig. 12. Lower relative difference is observed for the stoichiometric mixture while the scatter increases for lean and rich mixtures. Although CPM has been well characterized, there are still considerable uncertainties in LFS data measured using this method. To quantify the deviation of LFS measured by CPM in different

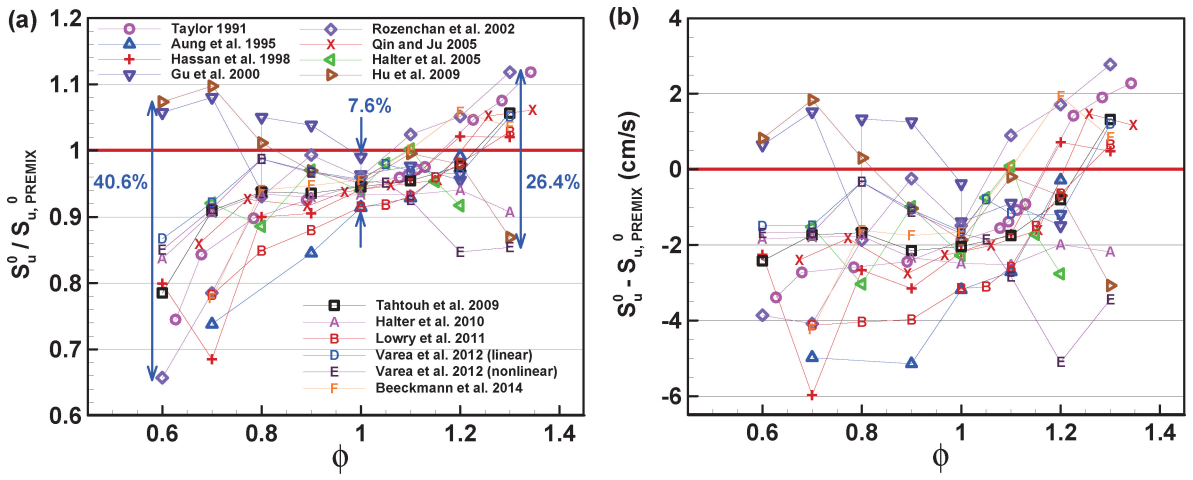

Figure 13 Deviation of S_u^0 measured by different groups from that predicted by simulation for the methane/air mixture at T_u = 298 K and P = 1 atm, $S_{u,PREMIX}^0$ based on GRI-Mech. 3.0. Figure adapted from [16].

experiments, Fig. 13 shows the relative difference between the measured LFS by CPM and the one predicted from PREMIX [26] when the GRI-Mech 3.0 [23] is used. For the stoichiometric mixture the relative difference between different experiments is 7.6% but it increases significantly and reaches 40.6% and 26.4% respectively for lean and rich mixtures.

Chen [16] reviewed different sources of uncertainty in LFS measurement using the CPM. The possible sources of uncertainty in CPM are mixture preparation [59, 102, 103], ignition [20, 42, 92, 104, 105], buoyancy [90, 106], confinement [15, 19, 21, 91], radiation [19, 61, 105, 107—109], extrapolation [13] and stretch [21].

For mixture preparation, while negligible uncertainty is anticipated from initial pressure variation, the uncertainty in LFS is around 2% for initial temperature variance of ±3 K and it reaches 2.5%—4% for initial temperature variance of ±5 K for methane/air at NTP [16]. The uncertainty in equivalence ratio strongly depends on the accuracy of the pressure gauge (usually the mixture is prepared using the partial pressure method). For methane/air at NTP and in lean and rich cases of ϕ=0.6 and 1.4, the uncertainty of LFS measurement is around 6% when pressure gauges with an accuracy of ±0.05% are used; while it reaches 10% when the normal pressure gauges with the accuracy of ±0.25% are used [16]. The ignition effect is negligible for LFS measurements when flame radii greater than 6 mm are used in data processing. However, the ignition effect becomes stronger for lower initial pressure [20, 42, 92, 104]. The buoyancy effect is negligible for mixtures with $S_u^0 > 15$ cm/s [106]; and it cannot be neglected for highly diluted mixtures for which micro-gravity experiments are needed [90]. As the optical access is provided in CPM, any instability developed in the flame front can be identified. The radiation effect increases greatly as LFS decreases [110]. For methane/air at NTP and with the equivalence ratio in the range of 0.7—1.3, the radiation-induced uncertainty in LFS measurement is within 3%. It reaches 5% for very lean or rich cases of ϕ=0.6 or 1.4. For near lean flammability mixtures ($0.5 < \phi < 0.6$), the radiation-induced uncertainty is above 6%.

In CPM, the zero burned gas velocity is assumed which is not valid for large flame radii. The negative burned gas velocity can be induced due to the confinement effect. Therefore, the upper flame radius used in data processing is limited by the confinement effect [21]. To diminish the confinement effect, usually flame radii with $R_f/R_W < 25\%$ are used in the data processing of the CPM. According to [16], for $R_f/R_W < 25\%$ the measured LFS by linear extrapolation is about 2% lower than its accurate value. The nonlinear stretch behavior also induces uncertainty in CPM. While for lean and stoichiometric methane/air mixtures the non-linear stretch behavior has a minor effect on S_u^0, the difference between linear and nonlinear models for rich methane/air mixtures can reach 15% [16]. The flame radius range used for extrapolation affects the influence of all above factors in CPM. The uncertainty originated from extrapolation to zero

stretch rate for methane/air at NTP around 4% for stoichiometric and lean premixtures, but it reaches more than 20% for $\phi=1.4$ [16].

Table 4 adapted from [16] summarizes all of the factors affecting the accuracy of LFS measurement for methane/air at NTP.

Table 4 Different factors affecting the uncertainty of LFS from CPM (The table is from [16])

Factors	Contributions to the uncertainty of LFS measured for methane/air at NTP using the CPM	Notes *
Initial P and T_u	Negligible contribution from P; around 2% for $\Delta T_u=\pm 3$ K; around 2.5%—4% for $\Delta T_u=\pm 5$ K.	P0, T0, N0
Composition (uncertainty in ϕ)	About 6% for $\phi=0.6$ and $\phi=1.4$ when pressure gauge with high accuracy of $\pm 0.05\%$ is used; significant discrepancy (above 10%) might be caused when pressure gauge with normal or low accuracy of $\pm 0.25\%$ is used.	P+, T0, N+
Ignition	Negligible contribution when $R_{fL}\geqslant 6$ mm.	P−, T−, N+
Buoyancy	Negligible contribution for $0.7\leqslant\phi\leqslant 1.4$.	P+, T−, N0
Instability	Negligible contribution.	P+, T0, N0
Confinement	Within 2%—3% for $R_f/R_W<25\%$; relatively large contribution when R_W is less than 8 cm.	P0, T0, N0
Radiation	Within 3% for $0.7\leqslant\phi\leqslant 1.3$; around 5% for $\phi=0.6$ and $\phi=1.4$; above 6% for near lean flammability mixtures ($0.5<\phi<0.6$).	P+, T−, N0
Nonlinear stretch behavior	Within 2% for $\phi\leqslant 1.0$; large contribution at high ϕ (it can be above 10% for $\phi=1.4$).	P−, T0, N+
Extrapolation (flame radius range)	Within 3～5% for $\phi\leqslant 1.0$; large contribution at high ϕ (it can be above 20% for $\phi=1.4$) when the linear model is used.	P−, T0, N+

* P0, T0, and N0 respectively indicate that the effect/contribution is nearly (not exactly) independent of initial pressure, initial temperature, and fuel carbon number (e.g. C_nH_{2n+2} for alkane); P+, T+, and N+ respectively indicate that the effect/contribution becomes larger at higher initial pressure, higher initial temperature, and higher fuel carbon number; and P−, T−, and N− respectively indicate that the effect/contribution becomes larger at lower initial pressure, lower initial temperature, and lower fuel carbon number.

Usually the combination of Eqs. (2) and (9) is used in CPM. However for the mixtures with two-stage heat release, positive burned gas velocity may exist and thereby Eq. (2) cannot be used. The two-stage heat release in nitromethane/air was studied in [111]. It was shown that the uncertainty in LFS exceeds 10% for some equivalence ratios. For the mixtures with low pressure and super adiabatic flame temperature, positive and negative burned gas velocities are induced and equilibrium density ratio cannot be used [112]. For stoichiometric methane/air at ambient temperature and initial pressure of 0.2 atm, the uncertainty of using Eq. (2) and (9) is 10%. For methane/oxygen at NTP and $\phi=3$, the uncertainty of using these equations is as large as 25%. Ref. [112] suggests to directly determine LFS by Eq. (10) in these mixtures.

3.2 Constant volume method (CVM)

The constant volume propagating spherical flame method (CVM) was first used in 1934 by Lewis and von Elbe [113]. In CVM, the evolution of chamber pressure rather than flame radius is recorded. Fig. 11 shows that the pressure rise is evident only when the flame radius is large enough. The pressure history is used to determine S_u^0 through correlations among S_u^0, pressure, and pressure rise rate. This method has the advantage that S_u^0 for a given mixture over a wide range of pressures and temperatures can be simultaneously measured by a single test [35]. Moreover, it is possible to use CVM to measure S_u^0 at engine-relevant pressures and temperatures of 50—70 atm and 600—800 K [69]. However, CVM has the disadvantage that the possible appearance of the flame instability is not identified and thereby the accuracy in LFS measurement may be reduced.

In CVM, the LFS is determined based on the following assumptions [35]: 1) the spherical flame front is smooth and free from instabilities; 2) both the unburned and burned gases are ideal; 3) the pressure is

uniformly distributed in the whole combustion vessel; 4) the unburned gas is compressed isentropically; 5) there is no dissociation or pre-flame reaction in the unburned gas; 6) chemical equilibrium is reached immediately after the flame front, and 7) the radiation and buoyancy effects are negligible.

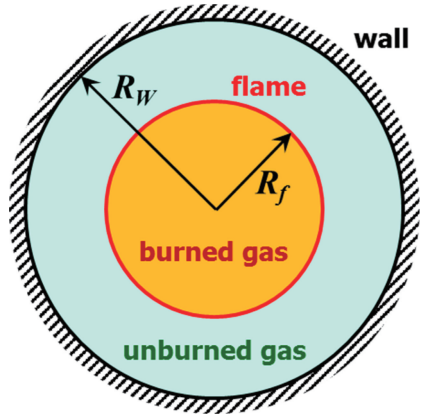

Figure 14 Schematic sketch of the spherical flame propagating in a closed spherical vessel.

Fig. 14 schematically shows the flame propagation in a closed spherical vessel. The spherical flame with the radius of R_f is assumed to be infinitely thin and it separates the burned and unburned gas regions. According to mass conservation, we have

$$m_0 = m_u + m_b, \tag{11}$$

where the subscripts 0, u and b denote the initial states and states of unburned and burned gases, respectively, and m stands for mass. From Eq. (11), we have

$$\frac{\mathrm{d}m_u}{\mathrm{d}t} = -\frac{\mathrm{d}m_b}{\mathrm{d}t}. \tag{12}$$

According to the definition of LFS, we have

$$\frac{\mathrm{d}m_u}{\mathrm{d}t} = -4\pi R_f^2 \rho_u S_u, \tag{13}$$

in which ρ_u is the density of unburned gas. The mass of unburned gas is $m_u = 4\pi(R_W^3 - R_f^3)\rho_u/3$, where R_W is the inner radius of the spherical chamber. Therefore, Eq. (13) becomes

$$S_u = \frac{\mathrm{d}R_f}{\mathrm{d}t} - \frac{R_W^3 - R_f^3}{3R_f^2\rho_u}\frac{\mathrm{d}\rho_u}{\mathrm{d}t}. \tag{14}$$

Since the unburned gas is compressed isentropically, we have

$$\rho_0/\rho_u = (P_0/P)^{1/\gamma_u}. \tag{15}$$

Substituting Eq. (15) into Eq. (14) yields

$$S_u = \frac{\mathrm{d}R_f}{\mathrm{d}t} - \frac{R_W^3 - R_f^3}{3P\gamma_u R_f^2}\frac{\mathrm{d}P}{\mathrm{d}t}. \tag{16}$$

The burned mass fraction (BMF) is defined as $x = m_b/m_0$. Therefore, Eq. (11) becomes

$$m_u = (1-x)m_0, \tag{17}$$

which indicates that

$$\frac{4\pi}{3}(R_W^3 - R_f^3)\rho_u = (1-x)\frac{4\pi}{3}R_W^3\rho_0. \tag{18}$$

Substituting Eq. (15) into Eq. (18) yields the following relationship between flame radius and pressure:

$$\frac{R_f}{R_W} = \left[1 - (1-x)\left(\frac{P_0}{P}\right)^{1/\gamma_u}\right]^{1/3}. \tag{19}$$

Substituting Eq. (19) into Eq. (16) yields

$$S_u = \frac{R_W}{3}\left[1 - (1-x)\left(\frac{P_0}{P}\right)^{1/\gamma_u}\right]^{-2/3}\left(\frac{P_0}{P}\right)^{1/\gamma_u}\frac{\mathrm{d}x}{\mathrm{d}t}, \tag{20}$$

which is widely used to determine S_u in CVM. In this equation, the BMF needs to be determined as a

function of pressure measured in experiments, i.e., $x=x(P)$.

Both experiments and simulations can be conducted to obtain LFS using CVM. However, direct numerical simulations of outwardly propagating spherical flames in a closed chamber with large pressure rise were only conducted by Chen and coworkers [21] and Egolfopoulos and coworkers [69]. Many groups have conducted the CVM experiments, including Metghalchi and coworkers [5, 49, 114—119], Stone and coworkers [48, 120—125] and Razus and coworkers [126—129]. Before 2001, Metghalchi's group only used a spherical chamber to measure the pressure evolution [5, 119] in the mixture. After 2001, they used both spherical and cylindrical vessels. The cylindrical vessel with optical access was used to identify possible instability and cellular formation in the flame front [49, 114—118]. Consequently, LFS obtained from the CVM was not affected by flame instability. Stone and coworkers used a spherical vessel with optical access so that both the pressure history and the flame front history were recorded in experiments [48, 120, 123]. Similar to Metghalchi's group, Stone's group used the flame front image to analyze flame instability and used the pressure history to get LFS. Razus and coworkers only measured the pressure history and no optical access was available in their spherical chamber [126, 129]. Table 5 summarizes the main groups used CVM experiments. Although many groups have used CVM to measure the LFS, there exists a considerable discrepancy among the LFS reported for the same mixture at the same initial condition. Fig. 15 shows the LFS of methane/air at NTP determined by CVM by different groups. The scatter between the reported data is considerable for different equivalence ratios.

Table 5 The characteristics of CVM experiments performed by different groups to measure LFS

Group	Vessel type and size
Manton et al. [130]	spherical, $R_W=7.65$ cm
Rallis et al. [131]	spherical, $R_W=8.01$ cm
Sharma et al. [132]	spherical, $R_W=6.94$ cm
Metghalchi and Keck [5, 119] [118]	spherical, $R_W=7.62$ cm
Metghalchi and coworkers [49, 114—117]	a) cylindrical chamber with optical access: to investigate shape of the flame b) spherical, $R_W=7.62$ cm to find LFS
Stone and coworkers [124]	spherical, $R_W=7.5$ cm
Stone and coworkers [48, 101, 120—122]	spherical, $R_W=8$ cm; with optical access
Razus and coworkers [127, 129]	spherical, $R_W=5$ cm
Matsugi et al. [133]	spherical, $R_W=7.65$ cm; with optical access
Egolfopoulos and coworkers [69]	a) cylindrical chamber with optical access b) spherical, $R_W=10.16$ cm to find LFS
Huzayyin et al. [50]	cylindrical, $R_W=7.2$ cm and L=15 cm
Kuznetsov et al. [93]	spherical, $R_W=12.5$ cm; with optical access
Farrel et al. [94]	spherical, $R_W=8.25$ cm; with optical access
Hill and Hung [47]	spherical, $R_W=8.25$ cm
Peters and coworkers [96, 97]	spherical, $R_W=5$ cm; with optical access
Takizawa et al. [45, 98, 134]	spherical, $R_W=9$ cm; with optical access
Fluixá et al. [99]	spherical, $R_W=20$ cm; with optical access
Dahoe [135]	cylindrical, $R_W=3.5$ cm and L=4.4 cm

The relative differences of normalized LFS measured by experiments for methane/air at NTP are compared in Fig. 16. The LFS calculated by PREMIX [23] is used for normalization. It is observed that the discrepancy among measured data is 18% for the stoichiometric mixture. It is noted that due to the lack of enough experimental data available at $\phi=0.6$ and 1.3, the experimental results are compared with simulation results. Comparing Fig. 16 with Fig. 13(a) around $\phi=1$ shows the discrepancy between reported LFS by CVM is higher than that measured by CPM.

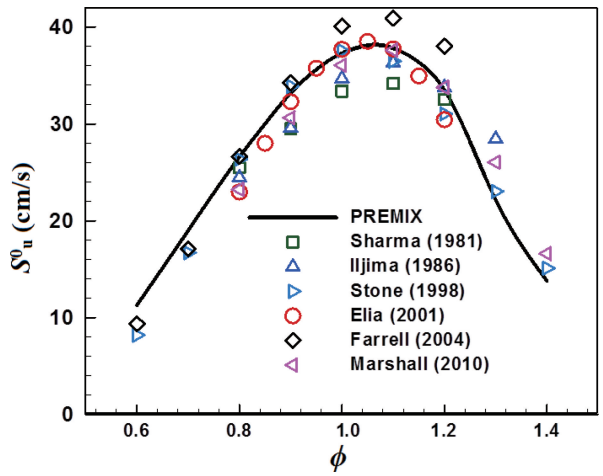

Figure 15 Laminar flame speed of methane/air at NTP. The symbols denote experimental results measured from CVM [94, 118, 122, 124, 132, 136]. The line denotes numerical results predicted by GRI-Mech. 3.0 [23] using PREMIX code [26]. Figure adapted from [70].

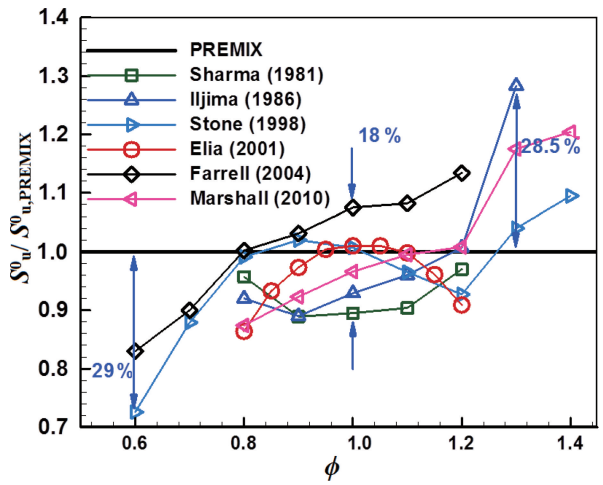

Figure 16 Deviation of S_u^0 measured by different groups [94, 118, 122, 124, 132, 136] from $S_{u,\mathrm{PREMIX}}^0$ predicted by simulation based on GRI-Mech. 3.0 [23]. Figure adapted from [70].

Due to the similarity between CVM and CPM, some of the uncertainty sources in CPM are also important in CVM. The possible sources of uncertainty in CVM are mixture preparation [59, 102, 103], instability [38, 87, 137], radiation [19, 61, 105, 107—109] and data processing. The uncertainty due to mixture preparation is similar for CVM and CPM which are summarized in Table 4. Since for CVM, data processing is conducted for flames with obvious pressure rise rate, the ignition effect is negligible and the buoyancy effect is less important compared to CPM. For CVM, the buoyancy effect is usually negligible for $S_u^0 > 15$ cm/s [106]. However, Takizawa et al. [98] found that the buoyancy effect is considerable for R-32 and R-32/134a mixtures whose LFS is less than 5 cm/s. For these mixtures, micro-gravity experiments need to be conducted.

In many experiments conducted by CVM, the optical access is not provided [126, 129, 138]. Therefore, the possible instability during the flame propagation is not revealed. In experiments conducted by CVM, the upper limit of the flame radius or pressure should be chosen to avoid the thermo-diffusive and hydrodynamic instabilities which enhance the flame propagation speed [87]. While the thermo-diffusive instability occurs for mixtures with negative Markstein length, the hydrodynamic instability occurs at high pressures where the flame thickness is very small [137]. The radiation effect decreases as LFS increases [110]. Therefore, the radiation induced uncertainty for the CVM is weaker than that for the CPM.

The most important factor affecting the accuracy of LFS measurement from CVM is data processing. There are different correlations among pressure, temperature, burned mass fraction and flame speed, which are used to obtain LFS. The performance of these correlations was reviewed in [70]. For stoichiometric methane/air at NTP, choosing an inappropriate correlation results in more than 10% uncertainty in LFS determination [70].

4 Summary and perspectives

Because of the importance of LFS, accurate determination of LFS is of great importance. The propagating spherical flame method is reviewed due to its advantage to measure the LFS at high pressures and evaluated temperatures. The recent advances in the constant pressure method (CPM) and constant volume method (CVM) based on propagating spherical flames are introduced here. The advantages of these methods together with their drawbacks are discussed.

Further studies are still needed in order to obtain accurate laminar flame speed from CPM and CVM. The possible topics of future research are:

1. Different factors inducing non-zero burned gas velocity and non-equilibrium density ratio were studied separately in CPM. However, the co-existence of these factors may further increase the uncertainty, which deserves further study.

2. The radiation effects have been extensively studied for the CPM [17, 109, 139, 140]. However, the radiation effects on the formulations used in CVM received little attention. For highly diluted mixtures with low flame speed the radiation effect in CVM may be considerable and thereby it needs further study.

3. Though the individual effects of different factors are well understood, it is still not clear how the coupling between different factors affects the accuracy of laminar flame speed measurement from CPM and CVM.

4. Recently, the cool flame has received great attention due to the need for understanding low-temperature chemistry and for developing advanced internal combustion engines [141—143]. However, it is difficult to accurately measure the LFS of a premixed cool flame. Such experiments should be developed since the LFS data of premixed cool flames are useful for developing low-temperature chemistry which has large uncertainty.

Acknowledgment

This work was supported by the National Natural Science Foundation of China (Grant Nos. 91741126, 91541204 and 51322602). Zheng Chen thanks helpful discussions with Professor Yiguang Ju at Princeton University.

References

[1] Summers D. Longman Dictionary of Contemporary English. Longman dictionaries, 1995.

[2] Key World Energy Statistics. International Energy Agency, 2016.

[3] Andrews G E, Bradley D. Determination of burning velocities: A critical review. Combust Flame, 1972, 18: 133—153.

[4] Law C K. Combustion Physics. Cambridge University Press, 2006.

[5] Metghalchi H, Keck J C. Laminar burning velocity of propane-air mixtures at high temperature and pressure. Combust Flame, 1980, 38: 143—154.

[6] Law C K, Sung C J, Wang H, et al. Development of comprehensive detailed and reduced reaction mechanisms for combustion modeling. AIAA Journal, 2003, 41: 1629—1646.

[7] Dooley S, Won S H, Chaos M, et al. A jet fuel surrogate formulated by real fuel properties. Combust Flame, 2010, 157: 2333—2339.

[8] Ranzi E, Frassoldati A, Grana R, et al. Hierarchical and comparative kinetic modeling of laminar flame speeds of hydrocarbon and oxygenated fuels. Prog Energy Combust Sci, 2012, 38: 468—501.

[9] Peters N. Turbulent Combustion. Cambridge University Press, 2000.

[10] Law C K. Fuel options for next-generation chemical propulsion. AIAA Journal, 2012, 50: 19—36.

[11] Li X, Hu E, Meng X, et al. Effect of Lewis number on nonlinear extrapolation methods from expanding spherical flames. Combust Sci Technol, 2017, 189: 1510—1526.

[12] Beeckmann J, Hesse R, Kruse S, et al. Propagation speed and stability of spherically expanding hydrogen/air flames: Experimental study and asymptotics. Proc Combust Inst, 2017, 36: 1531—1538.

[13] Jayachandran J, Lefebvre A, Zhao R, et al. A study of propagation of spherically expanding and counterflow laminar flames using direct measurements and numerical simulations. Proc Combust Inst, 2015, 35: 695—702.

[14] Varea E, Modica V, Renou B, et al. Pressure effects on laminar burning velocities and Markstein lengths for Isooctane-Ethanol-Air mixtures. Proc Combust Inst, 2013, 34: 735—744.

[15] Bonhomme A, Selle L, Poinsot T. Curvature and confinement effects for flame speed measurements in laminar spherical and cylindrical flames. Combust Flame, 2013, 160: 1208—1214.

[16] Chen Z. On the accuracy of laminar flame speeds measured from outwardly propagating spherical flames: Methane/air at normal temperature and pressure. Combust Flame, 2015, 162: 2442—2453.

[17] Chen Z. Effects of radiation absorption on spherical flame propagation and radiation-induced uncertainty in laminar flame speed measurement. Proc Combust Inst, 2017, 36: 1129—1136.

[18] Chen Z. On the extraction of laminar flame speed and Markstein length from outwardly propagating spherical flames. Combust Flame, 2011, 158: 291—300.

[19] Chen Z. Effects of radiation and compression on propagating spherical flames of methane/air mixtures near the lean flammability limit. Combust Flame, 2010, 157: 2267—2276.

[20] Chen Z, Burke M P, Ju Y G. Effects of Lewis number and ignition energy on the determination of laminar flame speed using propagating spherical flames. Proc Combust Inst, 2009, 32: 1253—1260.

[21] Chen Z, Burke M P, Ju Y. Effects of compression and stretch on the determination of laminar flame speeds using propagating spherical flames. Combust Theor Model, 2009, 13: 343—364.

[22] Chen Z. Effects of hydrogen addition on the propagation of spherical methane/air flames: A computational study. Int J Hydrogen Energy, 2009, 34: 6558—6567.

[23] Smith G, Golden D, Frenklach M, The GRI-Mech 3.0 chemical kinetic mechanism. http://combustion.berkeley.edu/gri-mech/.

[24] Li J, Zhao Z, Kazakov A, et al. An updated comprehensive kinetic model of hydrogen combustion. Int J Chem Kinet, 2004, 36: 566—575.

[25] Ji C, Dames E, Wang Y L, et al. Propagation and extinction of premixed C5—C12 n-alkane flames. Combust Flame, 2010, 157: 277—287.

[26] Kee R J, Grcar J, Smooke M, et al. PREMIX: a FORTRAN program for modeling steady laminar one-dimensional premixed flames. Sandia Report SAND85—8240, 1985.

[27] Lewis B, Von Elbe G. Combustion, Flames and Explosions of Gases. Elsevier, 2012.

[28] Tsuji H. Counterflow diffusion flames. Prog Energy Combust Sci, 1982, 8: 93—119.

[29] Wu C K, Law C K. On the determination of laminar flame speeds from stretched flames. Symp Int Combust Proc, 1985, 20: 1941—1949.

[30] Egolfopoulos F N, Cho P, Law C K. Laminar flame speeds of methane-air mixtures under reduced and elevated pressures. Combust Flame, 1989, 76: 375—391.

[31] Huang Y, Sung C J, Eng J A. Laminar flame speeds of primary reference fuels and reformer gas mixtures. Combust Flame, 2004, 139: 239—251.

[32] Levy A, Weinberg F. Optical flame structure studies: Some conclusions concerning the propagation of flat flames. Symp Int Combust Proc, 1958, 7: 296—303.

[33] Van Maaren A, Thung D S, De Goey L R H. Measurement of flame temperature and adiabatic burning velocity of methane/air mixtures. Combust Sci Technol, 1994, 96: 327—344.

[34] Qin X, Ju Y G. Measurements of burning velocities of dimethyl ether and air premixed flames at elevated pressures. Proc Combust Inst, 2005, 30: 233—240.

[35] Rallis C J, Garforth A M. The determination of laminar burning velocity. Prog Energy Combust Sci, 1980, 6: 303—329.

[36] Aung K T, Hassan M I, Faeth G M. Flame stretch interactions of laminar premixed hydrogen/air flames at normal temperature and pressure. Combust Flame, 1997, 109: 1—24.

[37] Brown M J, McLean I C, Smith D B, et al. Markstein lengths of CO/H2/air flames, using expanding spherical flames. Symp Int Combust Proc, 1996, 26: 875—881.

[38] Tse S D, Zhu D L, Law C K. Morphology and burning rates of expanding spherical flames in H_2/O_2/inert mixtures up to 60 atmospheres. Proc Combust Inst, 2000, 28: 1793—1800.

[39] Kwon S, Tseng L K, Faeth G M. Laminar burning velocities and transition to unstable flames in $H_2/O_2/N_2$ and $C_3H_8/O_2/N_2$ mixtures. Combust Flame, 1992, 90: 230—246.

[40] Aung K T, Hassan M I, Faeth G M. Effects of pressure and nitrogen dilution on flame/stretch interactions of laminar premixed H_2/O_2/

N_2 flames. Combust Flame, 1998, 112: 1—15.

[41] Bradley D, Hicks R A, Lawes M, et al. The measurement of laminar burning velocities and markstein numbers for iso-octane-air and iso-octane-n-heptane-air mixtures at elevated temperatures and pressures in an explosion bomb. Combust Flame, 1998, 115: 126—144.

[42] Huang Z, Zhang Y, Zeng K, et al. Measurements of laminar burning velocities for natural gas-hydrogen-air mixtures. Combust Flame, 2006, 146: 302—311.

[43] Chen Z, Qin X, Ju Y, et al. High temperature ignition and combustion enhancement by dimethyl ether addition to methane-air mixtures. Proc Combust Inst, 2007, 31: 1215—1222.

[44] Halter F, Chauveau C, Djebaïli-Chaumeix N, et al. Characterization of the effects of pressure and hydrogen concentration on laminar burning velocities of methane-hydrogen-air mixtures. Proc Combust Inst, 2005, 30: 201—208.

[45] Takizawa K, Takahashi A, Tokuhashi K, et al. Burning velocity measurement of fluorinated compounds by the spherical-vessel method. Combust Flame, 2005, 141: 298—307.

[46] Bradley D, Mitcheson A. Mathematical solutions for explosions in spherical vessels. Combust Flame, 1976, 26: 201—217.

[47] Hill P, Hung J. Laminar burning velocities of stoichiometric mixtures of methane with propane and ethane additives. Combust Sci Technol, 1988, 60: 7—30.

[48] Saeed K, Stone C R. Measurements of the laminar burning velocity for mixtures of methanol and air from a constant-volume vessel using a multizone model. Combust Flame, 2004, 139: 152—166.

[49] Parsinejad F, Arcari C, Metghalchi H. Flame structure and burning speed of JP-10 air mixtures. Combust Sci Technol, 2006, 178: 975—1000.

[50] Huzayyin A S, Moneib H A, Shehatta M S, et al. Laminar burning velocity and explosion index of LPG-air and propane-air mixtures. Fuel, 2008, 87: 39—57.

[51] Natarajan J, Lieuwen T, Seitzman J. Laminar flame speeds of H_2/CO mixtures: Effect of CO_2 dilution, preheat temperature, and pressure. Combust Flame, 2007, 151: 104—119.

[52] Bouvet N. Experimental and numerical studies of the fundamental flame speeds of methane/air and syngas (H_2/CO)/air mixtures. Université d'Orléans, 2009.

[53] Smith F A. Problems of stationary flames. Proc Combust Inst, 1948, 1: 206—219.

[54] Echekki T, Mungal M G. Flame speed measurements at the tip of a slot burner: Effects of flame curvature and hydrodynamic stretch. Symp Int Combust Proc, 1991, 23: 455—461.

[55] Law C K. Dynamics of stretched flames. Symp Int Combust Proc, 1989, 22: 1381—1402.

[56] Fu J, Tang C, Jin W, et al. Effect of preferential diffusion and flame stretch on flame structure and laminar burning velocity of syngas Bunsen flame using OH-PLIF. Int J Hydrogen Energy, 2014, 39: 12187—12193.

[57] Dagaut P, Karsenty F, Dayma G, et al. Experimental and detailed kinetic model for the oxidation of a Gas to Liquid (GtL) jet fuel. Combust Flame, 2014, 161: 835—847.

[58] He Y, Wang Z, Yang L, et al. Investigation of laminar flame speeds of typical syngas using laser based Bunsen method and kinetic simulation. Fuel, 2012, 95: 206—213.

[59] Egolfopoulos F N, Hansen N, Ju Y, et al. Advances and challenges in laminar flame experiments and implications for combustion chemistry. Prog Energy Combust Sci, 2014, 43: 36—67.

[60] Simmons R F, Wolfhard H G. Some limiting oxygen concentrations for diffusion flames in air diluted with nitrogen. Combust Flame, 1957, 1: 155—161.

[61] Jayachandran J, Zhao R, Egolfopoulos F N. Determination of laminar flame speeds using stagnation and spherically expanding flames: Molecular transport and radiation effects. Combust Flame, 2014, 161: 2305—2316.

[62] Bosschaart K J, de Goey L P H. Detailed analysis of the heat flux method for measuring burning velocities. Combust Flame, 2003, 132: 170—180.

[63] Botha J P, Spalding D B. The laminar flame speed of propane/air mixtures with heat extraction from the flame. Proc Math Phys Eng Sci, 1954, 225: 71—96.

[64] de Goey L P H, van Maaren A, Quax R M. Stabilization of adiabatic premixed laminar flames on a flat flame burner. Combust Sci Technol, 1993, 92: 201—207.

[65] Eng J A, Law C K, Zhu D L. On burner-stabilized cylindrical premixed flames in microgravity. Symp Int Combust Proc, 1994, 25: 1711—1718.

[66] Alekseev V A, Naucler J D, Christensen M, et al. Experimental uncertainties of the heat flux method for measuring burning velocities. Combust Sci Technol, 2016, 188: 853—894.

[67] Li B, Lindén J, Li Z S, et al. Accurate measurements of laminar burning velocity using the heat flux method and thermographic phosphor technique. Proc Combust Inst, 2011, 33: 939—946.

[68] Fiock E F, Marvin C F. The measurement of flame speeds. Chem Rev, 1937, 21: 367—387.

[69] Xiouris C, Ye T, Jayachandran J, et al. Laminar flame speeds under engine-relevant conditions: Uncertainty quantification and minimization in spherically expanding flame experiments. Combust Flame, 2016, 163: 270—283.

[70] Faghih M, Chen Z. The constant-volume propagating spherical flame method for laminar flame speed measurement. Sci Bull, 2016, 61: 1296—1310.

[71] Ellis O. Flame movement in gaseous explosive mixtures. Fuel, 1928, 7: 245—252.

[72] Kelley A P, Law C K. Nonlinear effects in the extraction of laminar flame speeds from expanding spherical flames. Combust Flame, 2009, 156: 1844—1851.

[73] Liang W, Wu F, Law C K. Extrapolation of laminar flame speeds from stretched flames: Role of finite flame thickness. Proc Combust Inst, 2017, 36: 1137—1143.

[74] Kelley A P, Bechtold J K, Law C K. Premixed flame propagation in a confining vessel with weak pressure rise. J Fluid Mech, 2011, 691: 26—51.

[75] Wu F, Liang W, Chen Z, et al. Uncertainty in stretch extrapolation of laminar flame speed from expanding spherical flames. Proc Combust Inst, 2015, 35: 663—670.

[76] Varea E, Beeckmann J, Pitsch H, et al. Determination of burning velocities from spherically expanding H2/air flames. Proc Combust Inst, 2015, 35: 711—719.

[77] Varea E, Modica V, Vandel A, et al. Measurement of laminar burning velocity and Markstein length relative to fresh gases using a new postprocessing procedure: application to laminar spherical flames for methane, ethanol and isooctane/air mixtures. Combust Flame, 2012, 159: 577—590.

[78] Halter F, Tahtouh T, Mounaïm-Rousselle C. Nonlinear effects of stretch on the flame front propagation. Combust Flame, 2010, 157: 1825—1832.

[79] Tahtouh T, Halter F, Mounaïm-Rousselle C. Measurement of laminar burning speeds and Markstein lengths using a novel methodology. Combust Flame, 2009, 156: 1735—1743.

[80] Brequigny P, Dayma G, Halter F, et al. Laminar burning velocities of premixed nitromethane/air flames: An experimental and kinetic modeling study. Proc Combust Inst, 2015, 35: 703—710.

[81] Galmiche B, Halter F, Foucher F, et al. Effects of dilution on Laminar burning velocity of premixed methane/air flames. Energy Fuels, 2011, 25: 948—954.

[82] Cai L, Minwegen H, Beeckmann J, et al. Experimental and numerical study of a novel biofuel: 2-Butyltetrahydrofuran. Combust Flame, 2017, 178: 257—267.

[83] Burke U, Beeckmann J, Kopp W A, et al. A comprehensive experimental and kinetic modeling study of butanone. Combust Flame, 2016, 168: 296—309.

[84] Beeckmann J, Cai L, Pitsch H. Experimental investigation of the laminar burning velocities of methanol, ethanol, n-propanol, and n-butanol at high pressure. Fuel, 2014, 117, Part A: 340—350.

[85] Kelley A P, Smallbone A J, Zhu D L, et al. Laminar flame speeds of C5 to C8 n-alkanes at elevated pressures: Experimental determination, fuel similarity, and stretch sensitivity. Proc Combust Inst, 2011, 33: 963—970.

[86] Yang S, Yang X, Wu F, et al. Laminar flame speeds and kinetic modeling of H2/O2/diluent mixtures at sub-atmospheric and elevated pressures. Proc Combust Inst, 2017, 36: 491—498.

[87] Bradley D, Lawes M, Liu K, et al. Laminar burning velocities of lean hydrogen-air mixtures at pressures up to 1.0 MPa. Combust Flame, 2007, 149: 162—172.

[88] Hassan M I, Aung K T, Faeth G M. Measured and predicted properties of laminar premixed methane/air flames at various pressures. Combust Flame, 1998, 115: 539—550.

[89] Hassan M I, Aung K T, Kwon O C, et al. Properties of laminar premixed hydrocarbon/air flames at various pressures. J Propul Power, 1998, 14: 479—488.

[90] Qiao L, Gu Y, Dahm W J A, et al. Near-limit laminar burning velocities of microgravity premixed hydrogen flames with chemically-passive fire suppressants. Proc Combust Inst, 2007, 31: 2701—2709.

[91] Burke M P, Chen Z, Ju Y, et al. Effect of cylindrical confinement on the determination of laminar flame speeds using outwardly propagating flames. Combust Flame, 2009, 156: 771—779.

[92] Kim H H, Won S H, Santner J, et al. Measurements of the critical initiation radius and unsteady propagation of n-decane/air premixed flames. Proc Combust Inst, 2013, 34: 929—936.

[93] Kuznetsov M, Redlinger R, Breitung W, et al. Laminar burning velocities of hydrogen-oxygen-steam mixtures at elevated temperatures and pressures. Proc Combust Inst, 2011, 33: 895—903.

[94] Farrell J, Johnston R, Androulakis I. Molecular structure effects on laminar burning velocities at elevated temperature and pressure. SAE Technical Paper, 2004, doi:10.4271/2004-01-29362004-2001-2936.

[95] Daly C A, Simmie J M, Würmel J, et al. Burning velocities of dimethyl ether and air. Combust Flame, 2001, 125: 1329—1340.

[96] Jerzembeck S, Glawe C, Keppner J, et al. Laminar burning velocities from Schlieren-and pressure history measurements. 5th WSEAS International Conference on Fluid Mechanics (FLUIDS'08) Acapulco, Mexico, January, 2008, 25—27.

[97] Jerzembeck S, Peters N, Pepiot-Desjardins P, et al. Laminar burning velocities at high pressure for primary reference fuels and gasoline: Experimental and numerical investigation. Combust Flame, 2009, 156: 292—301.

[98] Takizawa K, Takagi S, Tokuhashi K, et al. Assessment of burning velocity test methods for mildly flammable refrigerants, Part 1: Closed-vessel method. Ashrae Tran, 2013, 119: 243—254.

[99] Fluixá F V T, Olavarría B G, Hoyos D I, et al. Experimental determination of the burning velocity of mixtures of n-heptane and toluene in engine-like conditions. Flow, Turbulence and Combustion, 2012, 89: 183—213.

[100] Pizzuti L, Martins C A, dos Santos L R, et al. Laminar burning velocity of methane/air mixtures and flame propagation speed close to the chamber wall. Energy Procedia, 2017, 120: 126—133.

[101] Hinton N, Stone R, Cracknell R. Laminar burning velocity measurements in constant volume vessels - Reconciliation of flame front imaging and pressure rise methods. Fuel, 2018, 211: 446—457.

[102] Santner J, Haas F M, Dryer F L, et al. High temperature oxidation of formaldehyde and formyl radical: A study of 1,3,5-trioxane laminar burning velocities. Proc Combust Inst, 2015, 35: 687—694.

[103] Li X, You X, Wu F, et al. Uncertainty analysis of the kinetic model prediction for high-pressure H2/CO combustion. Proc Combust Inst, 2015, 35: 617—624.

[104] Bradley D, Gaskell P H, Gu X J. Burning velocities, markstein lengths, and flame quenching for spherical methane-air flames: A computational study. Combust Flame, 1996, 104: 176—198.

[105] Beeckmann J, Chaumeix N, Dagaut P, et al. Collaborative study for accurate measurements of laminar burning velocity. Proceedings of the European Combustion Meeting, 2013, 3—76.

[106] Ronney P D, Wachman H Y. Effect of gravity on laminar premixed gas combustion I: Flammability limits and burning velocities. Combust Flame, 1985, 62: 107—119.

[107] Chen Z, Qin M, Xu B, et al. Studies of radiation absorption on flame speed and flammability limit of CO_2 diluted methane flames at elevated pressures. Proc Combust Inst, 2007, 31: 2693—2700.

[108] Santner J, Haas F M, Ju Y G, et al. Uncertainties in interpretation of high pressure spherical flame propagation rates due to thermal radiation. Combust Flame, 2014, 161: 147—153.

[109] Yu H, Han W, Santner J, et al. Radiation-induced uncertainty in laminar flame speed measured from propagating spherical flames. Combust Flame, 2014, 161: 2815—2824.

[110] Yu H, Chen Z. End-gas autoignition and detonation development in a closed chamber. Combust Flame, 2015, 162: 4102—4111.

[111] Faghih M, Chen Z. Two-stage heat release in nitromethane/air flame and its impact on laminar flame speed measurement. Combust Flame, 2017, 183: 157—165.

[112] Faghih M, Chen Z. On the measurement of laminar flame speed from low-pressure and super-adiabatic propagating spherical flames. Proc Combust Inst, 2018, in press. https://doi.org/10.1016/j.proci.2018.05.027.

[113] Lewis B, Von Elbe G. Determination of the speed of flames and the temperature distribution in a spherical bomb from time-pressure explosion records. J Chem Phys, 1934, 2: 283—290.

[114] Moghaddas A, Bennett C, Rokni E, et al. Laminar burning speeds and flame structures of mixtures of difluoromethane (HFC-32) and 1,1-difluoroethane (HFC-152a) with air at elevated temperatures and pressures. HVAC&R Res, 2014, 20: 42—50.

[115] Moghaddas A, Eisazadeh-Far K, Metghalchi H. Laminar burning speed measurement of premixed n-decane/air mixtures using spherically expanding flames at high temperatures and pressures. Combust Flame, 2012, 159: 1437—1443.

[116] Eisazadeh-Far K, Moghaddas A, Al-Mulki J, et al. Laminar burning speeds of ethanol/air/diluent mixtures. Proc Combust Inst, 2011, 33: 1021—1027.

[117] Rahim F, Elia M, Ulinski M, et al. Burning velocity measurements of methane-oxygen-argon mixtures and an application to extend methane-air burning velocity measurements. Int J Engine Res, 2002, 3: 81—92.

[118] Elia M, Ulinski M, Metghalchi H. Laminar burning velocity of methane-air-diluent mixtures. J Eng Gas Turb Power, 2001, 123: 190—196.

[119] Metghalchi H, Keck J C. Burning velocities of mixtures of air with methanol, isooctane, and indolene at high pressure and temperature. Combust Flame, 1982, 48: 191—210.

[120] Hinton N, Stone R. Laminar burning velocity measurements of methane and carbon dioxide mixtures (biogas) over wide ranging temperatures and pressures. Fuel, 2014, 116: 743—750.

[121] Marshall S P, Taylor S, Stone C R, et al. Laminar burning velocity measurements of liquid fuels at elevated pressures and temperatures with combustion residuals. Combust Flame, 2011, 158: 1920—1932.

[122] Marshall S P, Stone R, Heghes§ C, et al. High pressure laminar burning velocity measurements and modelling of methane and n-butane. Combust Theor Model, 2010, 14: 519—540.

[123] Saeed K, Stone C R. The modelling of premixed laminar combustion in a closed vessel. Combust Theor Model, 2004, 8: 721—743.

[124] Stone R, Clarke A, Beckwith P. Correlations for the laminar-burning velocity of methane/diluent/air mixtures obtained in free-fall experiments. Combust Flame, 1998, 114: 546—555.

[125] Clarke A, Stone R, Beckwith P. Measuring the laminar burning velocity of methane/diluent/air mixtures within a constant-volume combustion bomb in a micro-gravity environment. J Inst Energ, 1995, 68: 130—136.

[126] Mitu M, Razus D, Giurcan V, et al. Normal burning velocity and propagation speed of ethane-air: Pressure and temperature

dependence. Fuel, 2015, 147: 27—34.
[127] Mitu M, Razus D, Giurcan V, et al. Experimental and numerical study of laminar burning velocity of ethane-air mixtures of variable initial composition, temperature and pressure. Energy Fuels, 2014, 28: 2179—2188.
[128] Giurcan V, Razus D, Mitu M, et al. Numerical study of the laminar flame propagation in ethane-air mixtures. Open Chemistry, 2014, 12: 391—402.
[129] Razus D, Brinzea V, Mitu M, et al. Burning velocity of propane-air mixtures from pressure-time records during explosions in a closed spherical vessel. Energy Fuels, 2012, 26: 901—909.
[130] Manton J, von Elbe G, Lewis B. Burning-velocity measurements in a spherical vessel with central ignition. Symp Int Combust Proc, 1953, 4: 358—363.
[131] Rallis C J, Garforth A M, Steinz J A. Laminar burning velocity of acetylene-air mixtures by the constant volume method: Dependence on mixture composition, pressure and temperature. Combust Flame, 1965, 9: 345—356.
[132] Sharma S P, Agrawal D D, Gupta C P. The pressure and temperature dependence of burning velocity in a spherical combustion bomb. Symp Int Combust Proc, 1981, 18: 493—501.
[133] Matsugi A, Shiina H, Takahashi A, et al. Burning velocities and kinetics of H2/NF3/N2, CH4/NF3/N2, and C3H8/NF3/N2 flames. Combust Flame, 2014, 161: 1425—1431.
[134] Takizawa K, Takahashi A, Tokuhashi K, et al. Burning velocity measurement of HFC-41, HFC-152, and HFC-161 by the spherical-vessel method. J Fluorine Chem, 2006, 127: 1547—1553.
[135] Dahoe A E. Laminar burning velocities of hydrogen-air mixtures from closed vessel gas explosions. J Loss Prev Process Ind, 2005, 18: 152—166.
[136] Iijima T, Takeno T. Effects of temperature and pressure on burning velocity. Combust Flame, 1986, 65: 35—43.
[137] Jomaas G, Law C K, Bechtold J K. On transition to cellularity in expanding spherical flames. J Fluid Mech, 2007, 583: 1—26.
[138] Movileanu C, Brinzea V, Mitu M, et al. Explosion pressures of confined deflagrations propogating in stoichiometric gaseous mixtures of lower alkanes with air. Analele Universitatii Bucuresti: Chimie, 2009, 18: 39—46.
[139] Chen Z. Effects of radiation on large-scale spherical flame propagation. Combust Flame, 2017, 183: 66—74.
[140] Sohn C H, Chen Z, Ju Y. Effects of radiation on the uncertainty of flame speed determination using spherically propagating flames with $CO/CO_2/H_2O$ dilutions at elevated pressures. Int J Heat Mass Transfer, 2015, 86: 820—825.
[141] Ju Y, Reuter C B, Won S H. Numerical simulations of premixed cool flames of dimethyl ether/oxygen mixtures. Combust Flame, 2015, 162: 3580—3588.
[142] Ju Y. On the propagation limits and speeds of premixed cool flames at elevated pressures. Combust Flame, 2017, 178: 61—69.
[143] Zhang W, Faghih M, Gou X, et al. Numerical study on the transient evolution of a premixed cool flame. Combust Flame, 2018, 187: 129—136.

CHEN Zheng

Dr. CHEN Zheng(陈正) is a researcher at the College of Engineering, Peking University. He received his B. E and M. E degrees from Tsinghua University in 2001 and 2003, respectively, and Ph. D degree from Princeton University in 2009. His current research focuses on flame dynamics of laminar premixed flame, flames with low-temperature chemistry, and autoignition and detonation development. He has been awarded the Bernard Lewis Fellowship from the Combustion Institute, and the Young Investigator Prize from Asian-Pacific Conference on Combustion. He is on the editorial board of *Combustion and Flame* (2017—2022) and *Chinese Journal of Aeronautics* (2017—2020). He is the Program Co-Chair for China National Symposium on Combustion in 2017 and 2018, and the Colloquium Co-Chair for Laminar Flames of the 36th and 37th International Symposium on Combustion.